Shape-tailorable High-energy Asymmetric Micro-supercapacitors based on Plasma Reduced and Nitrogen-doped Graphene Oxide and MoO_2 Nanoparticles

Liangzhu zhang,[a⊥], Zhiqiang Chen,[a⊥] Shuanghao Zheng,[bc] Si Qin,[a] Jiemin Wang,[a] Cheng Chen,[a] Dan Liu,[a] Lifeng Wang,[a] Guoliang Yang,[a] Yuyu Su,[a] Zhong-Shuai Wu,*[b] Xinhe Bao,[b] Joselito Razal,[a] and Weiwei Lei,*[a]*

[a] Institute for Frontier Materials, Deakin University, Waurn Ponds Campus, Locked Bag 20000, Victoria 3220, Australia.

E-mail: dan.liu@deakin.edu.au; weiwei.lei@deakin.edu.au

[b] Dalian National Laboratory for Clean Energy, Dalian Institute of Chemical Physics, Chinese Academy of Sciences, 457 Zhongshan Road, Dalian 116023, China.

E-mail: wuzs@dicp.ac.cn

[c] University of Chinese Academy of Sciences, 19 A Yuquan Rd, Shijingshan District, Beijing, 100049, China.

Calculation

The capacitance values were calculated from the discharge curves of CV and GCD according to the following equations (1) and (2):

$$C = \frac{1}{\nu(V_f - V_i)} \int_{V_i}^{V_f} I(V)dV \quad (1)$$

$$C = \frac{I\Delta t}{(V_f - V_i)} \quad (2)$$

Where ν is the scan rate (V s^{-1}), V_f and V_i are the potential limits of CV curve. $I(V)$ is the voltammetry discharge current (A). Δt refers to the discharge time (s).

Areal capacitance (mF cm^{-2}) and volumetric capacitance (F cm^{-3}) of the devices were calculated based on area and volume of two electrodes according to the formula (3) and (4):

$$C_{device}^{areal} = C/A_{electrode} \quad (3)$$

$$C_{device}^{volumetric} = C/A_{electrode} \quad (4)$$

The volumetric energy density E (Wh cm^{-3}) and power density P (W cm^{-3}) of the device was obtained from the equations:

$$E = \frac{1}{2} \times C_{device}^{volumetric} \times \frac{(V_f - V_i - IR)^2}{3600} \quad (5)$$

$$P = \frac{E}{\Delta t} \times 3600 \quad (6)$$

Where IR is Ohmic drop

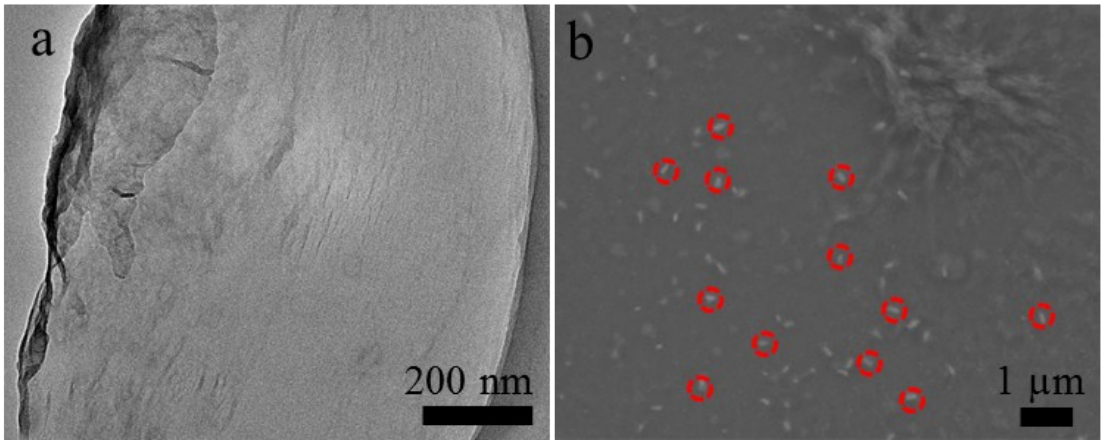

Figure S1. Morphology of GO nanosheet and GO-MoO_2 composite. (a) A typical TEM image of GO nanosheet. (b) SEM image of GO-MoO_2 nanocomposite on a polished Si substrate, exhibiting MoO_2 nanoparticles uniformly dispersed in GO nanosheet.

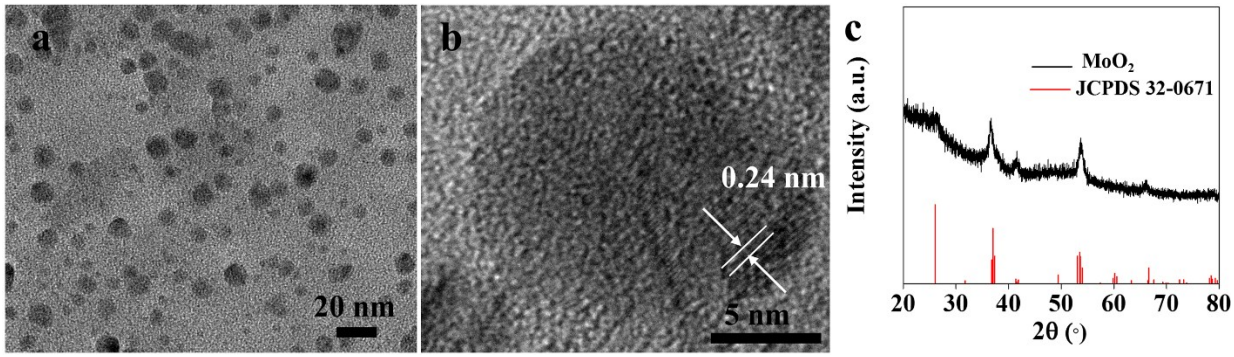

Figure S2. Morphology of MoO_2 nanoparticles. (a) TEM image of MoO_2 nanoparticles, showing the nanoparticle with uniform size of 5-10 nm. (b) HRTEM image of MoO_2 nanoparticles. The fringes with a distance of 0.24 nm is assigned to lattice plane of (211). (c) X-ray diffraction of MoO_2 nanoparticles, the diffraction peaks are in good agreement with the standard card of JCPDS 32-0671.

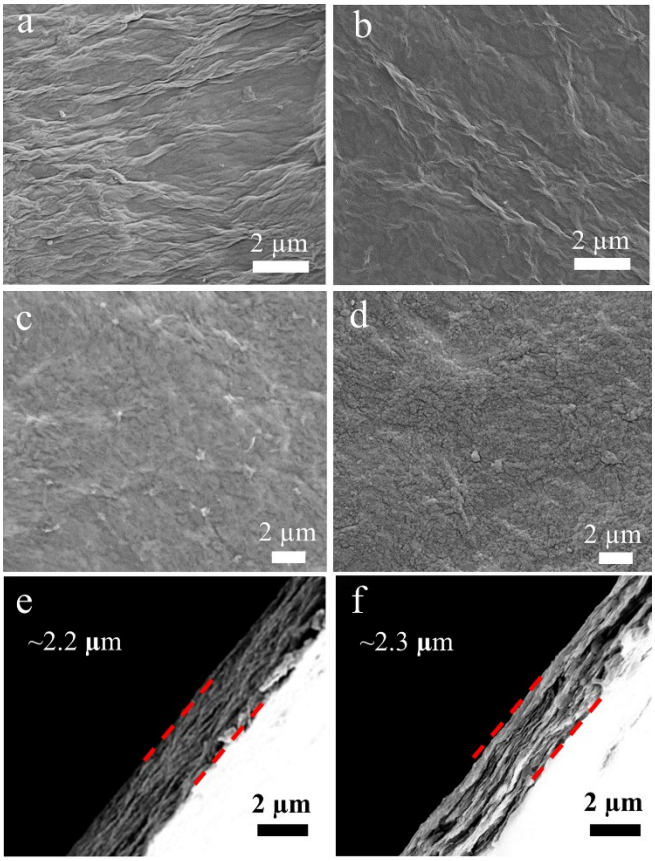

Figure S3. Morphologies of GO, PNG, GO-MoO_2 and PNG-MoO_2 films. (a, b) SEM images of top surface of GO and PNG films, showing the uniform and flat morphologies. (c, d) SEM images of top surface of GO-MoO_2 and PNG- MoO_2 films. (e, f) Cross-section SEM images of PNG film with a thickness of 2.2 μm and PNG-MoO_2 film with a thickness of 2.3 μm.

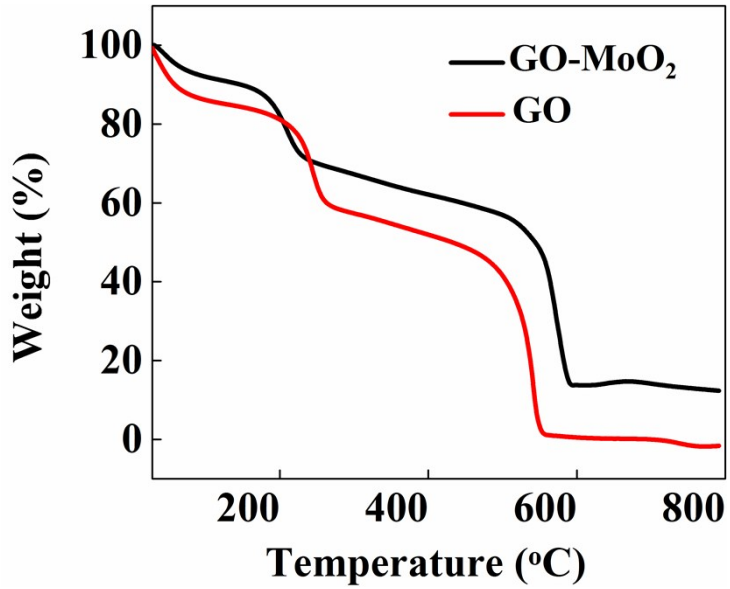

Figure S4. TGA curves of GO and GO-MoO_2 films in air. GO exhibits about 10 wt. % loss below 100 °C and more than 41 wt. % loss at around 240 °C, resulting from the removal of residue water and labile oxygen-containing functional groups, respectively. A significant drop in mass of GO around 600 °C is due to the bulk pyrolysis of the carbon. Similar trends were observed in GO-MoO_2 composite film but 13 wt. % remained due to the weight content of MoO_2.

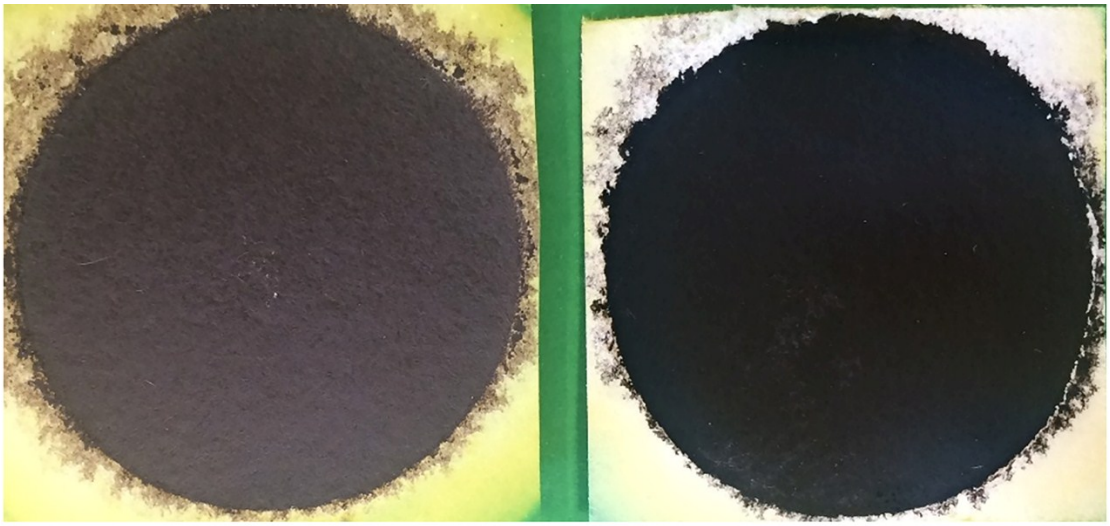

Figure S5. Photo images of GO (left) and PNG (right), which show the colour of GO changes from yellow brown to dark black after plasma treatment.

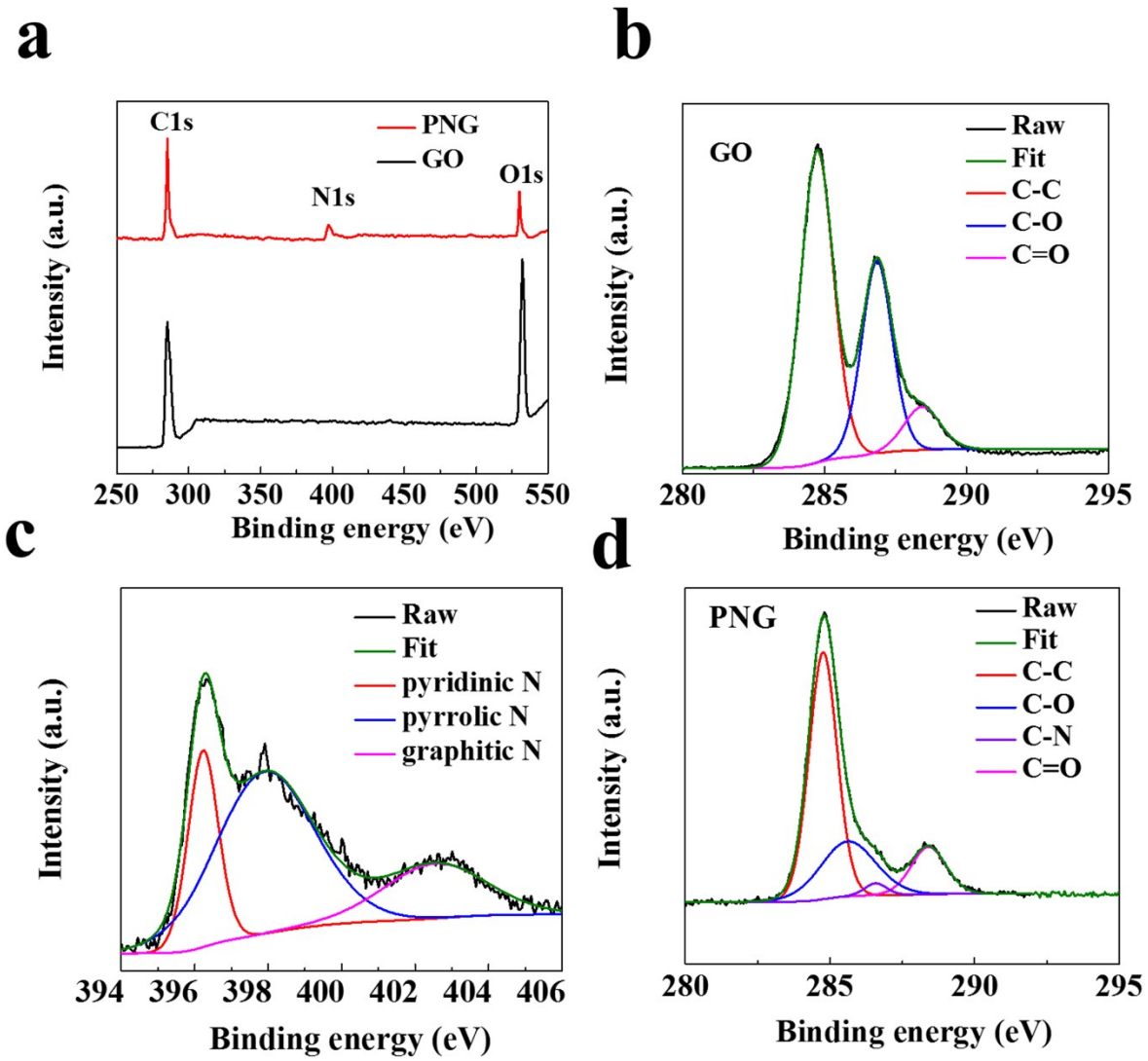

Figure S6. (a) XPS survey spectra of GO and PNG films. It shows that plasma reduction on GO films generates a large decrease in the atomic content of oxygen (530 eV) and carbon (284.7 eV). The O/C ratio decreased from 0.40 to 0.18. The N-doping with 8.05 at% concentration occurred in PNG film. (b, d) High resolution C1s XPS spectra of GO and PNG film. It shows a new generated C-N bond in PNG figure where the intensity of oxygen-base groups reduced, indicating the effective reduction after plasma treatment. (c) High resolution N1s XPS spectra of PNG film, the N1s peak can be separated into three peaks, which can be assigned to pyridinic (396.2 eV), pyrrolic (397.9 eV) and graphitic N (402.5 eV).

Table S1. XPS survey data of the GO and PNG films.

Sample	Relative Atomic Percentage (%)			O/C Atomic Ratios
	C1s	O1s	N1s	
GO	71.43	28.57	0	0.40
PNG	77.92	14.03	8.05	0.18

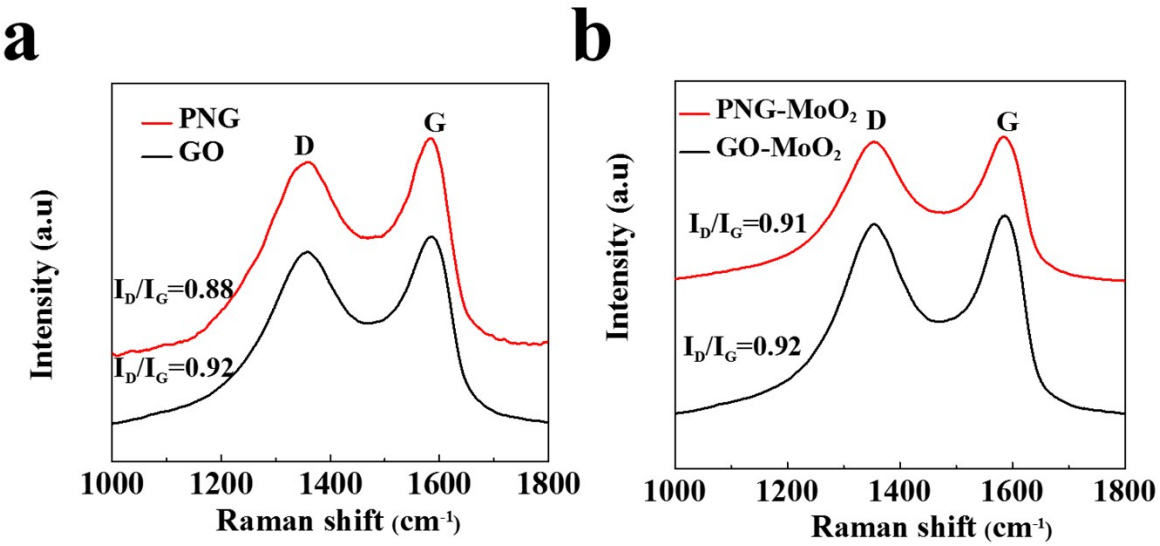

Figure S7. Raman spectra for (a) GO and PNG films, (b) GO-MoO_2 and PNG-MoO_2 films. Two distinguished peaks at 1353 cm^{-1} and 1585 cm^{-1} belong to D-band and G-band of GO, respectively. The intensity ratio (I_D/I_G) of both GO and GO-MoO_2 are about 0.92, while the I_D/I_G of PNG and PNG-MoO_2 are 0.88 and 0.91, respectively. The decrease of I_D/I_G after plasma reduction, indicates the reduced defects or disorder in reduced films, which may result from the plasma cleaning and repairing of carbon networks.[1]

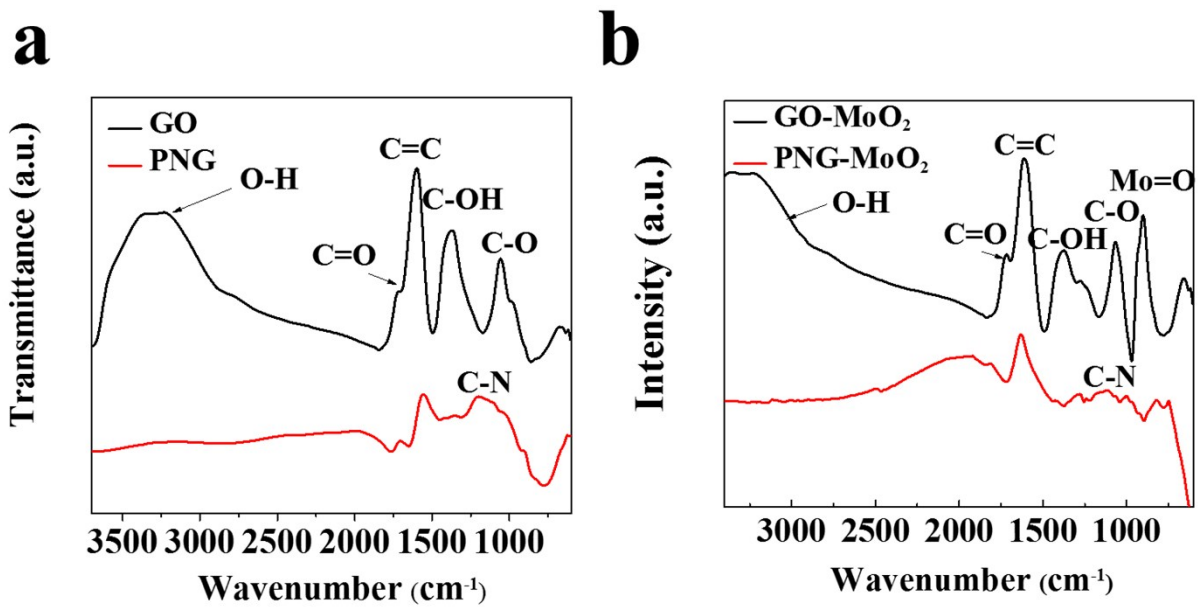

Figure S8. FTIR spectra for (a) GO and PNG films, (b) GO-MoO_2 and PNG-MoO_2 films. The peaks at 3000-3500 cm^{-1} are related to O-H vibrations originating from hydroxyl groups or water. The peaks at 1730 cm^{-1} and 1595 cm^{-1} can be attributed to C=O and C=C stretching. The peaks at 1430 cm^{-1} and 1085 cm^{-1} originate from O-H vibrations and C-O bond, and the shoulder peak at 970 cm^{-1} arises from epoxide, ether, and peroxide groups. After N_2/H_2 plasma treatment, most of these peaks were weakened, indicating that plasma reduction is effective at removing oxygen-containing groups. The additional peak at 1200 cm^{-1} is attributed to newly formed C-N bonding indicating the successful N-doping in PNG and PNG-MoO_2 films.[2]

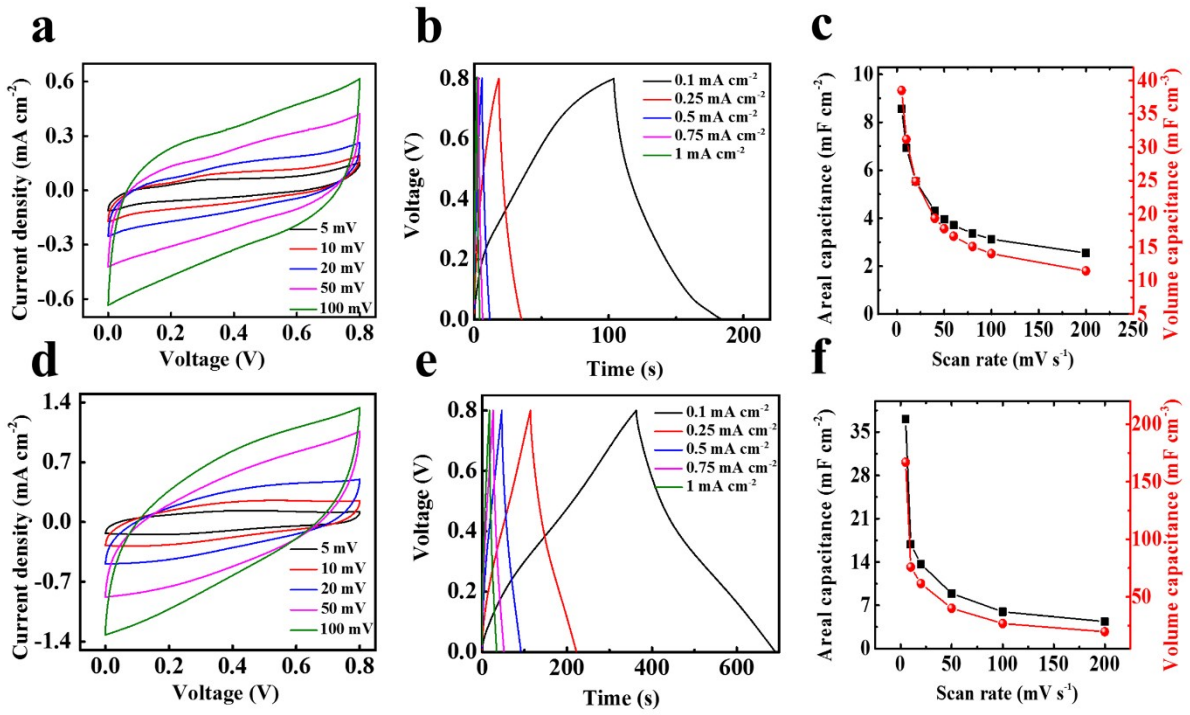

Figure S9. Electrochemical characterization of RGO-MSCs and PNG-MSCs. (a) CV curves of RGO-MSCs at a scan rate of 5 mV/s to 100 mV/s. (B) GCD curves of RGO-MSCs at various current densities from 0.1 to 1 mA cm^{-2}. (c) Areal capacitance and volumetric capacitance of RGO-MSCs under different scan rate. (d) CV curves of PNG-MSCs at a scan rate of 5 mV/s to 100 mV/s. (e) GCD curves of PNG-MSCs at various current densities from 0.1 to 1 mA cm^{-2}.(f) Areal capacitance and volumetric capacitance of PNG-MSCs under different scan rate.

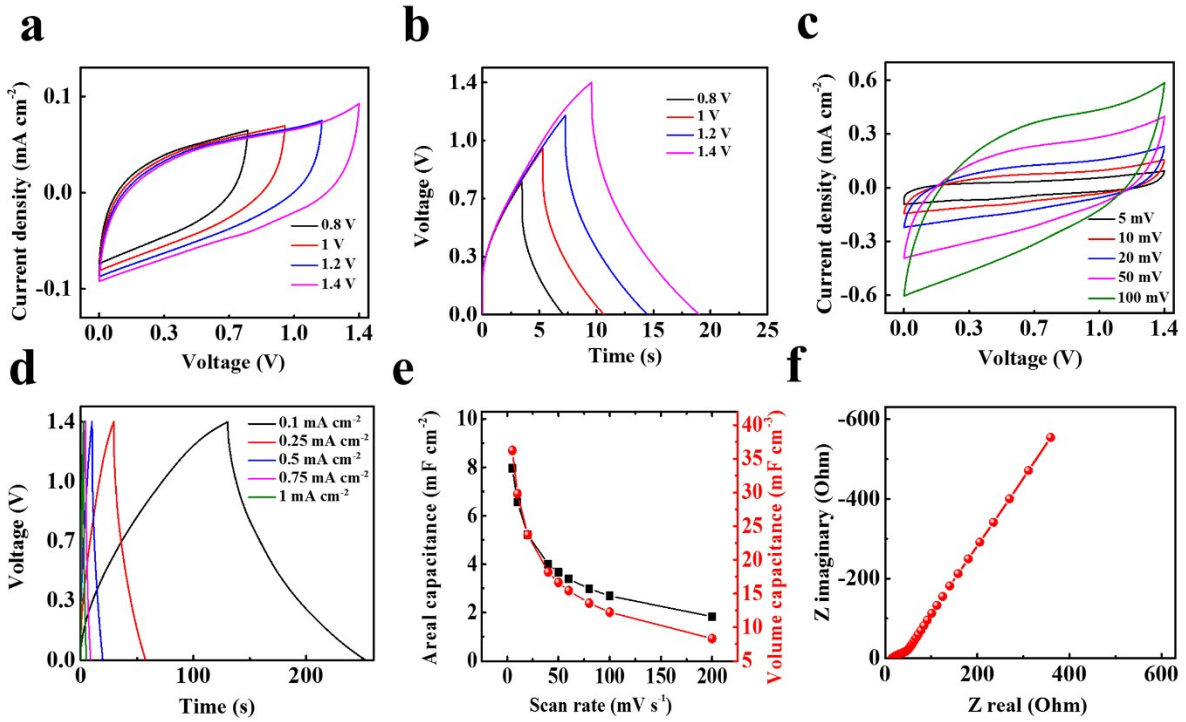

Figure S10. Electrochemical characterization of in-plane RGO//RGO-MoO_2-AMSCs. (a) CV curves RGO//RGO-MoO_2-AMSCs under different applied voltages from 0.8 to 1.4 V at a scan rate of 5 mV/s. (b) GCD curves with different voltages at a current density of 0.5 mA/cm^2. (c) CV curves obtained at different scan rates from 5 to 100 mV s^{-1}. (d) GCD curves obtained at various current densities from 0.1 to 1 mA cm^{-2}. (e) Areal capacitance and volumetric capacitance of RGO//RGO-MoO_2-AMSCs. (f) Complex plane plots of RGO//RGO-MoO_2-AMSCs.

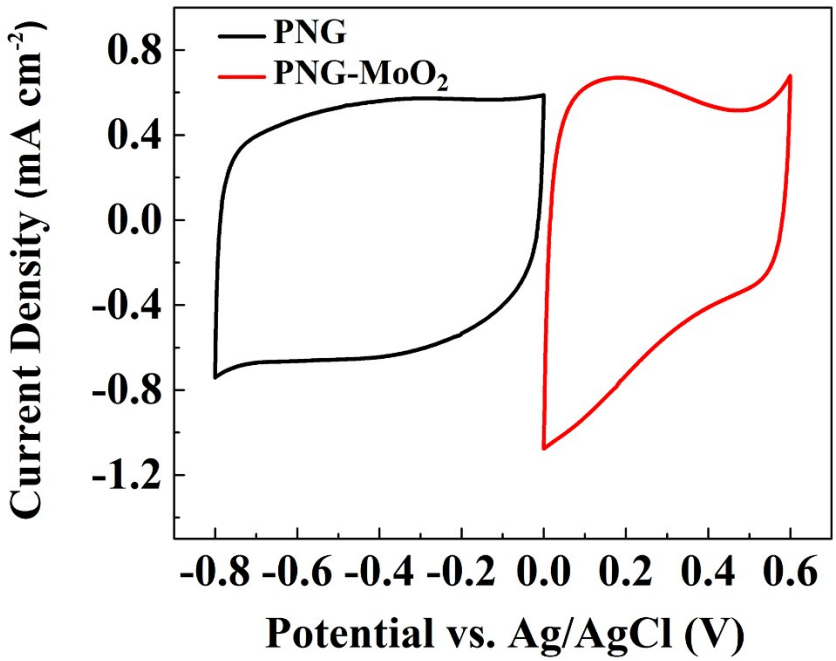

Figure S11. CV curves of PNG and PNG-MoO_2 films at a scan rate of 5 mV/s in a three-electrode configuration in 1M LiCl solution, using Ag/AgCl as reference electrode and Pt foil as counter electrode. The operating potential windows for PNG film and PNG-MoO_2 film are -0.8-0 V and 0-0.6 V, respectively. It is calculated that the optimal area ratio of PNG and PNG-MoO_2 is 1:1. Thus, the PNG//PNG-MoO_2-AMSCs can deliver a maximum working voltage up to 1.4 V.

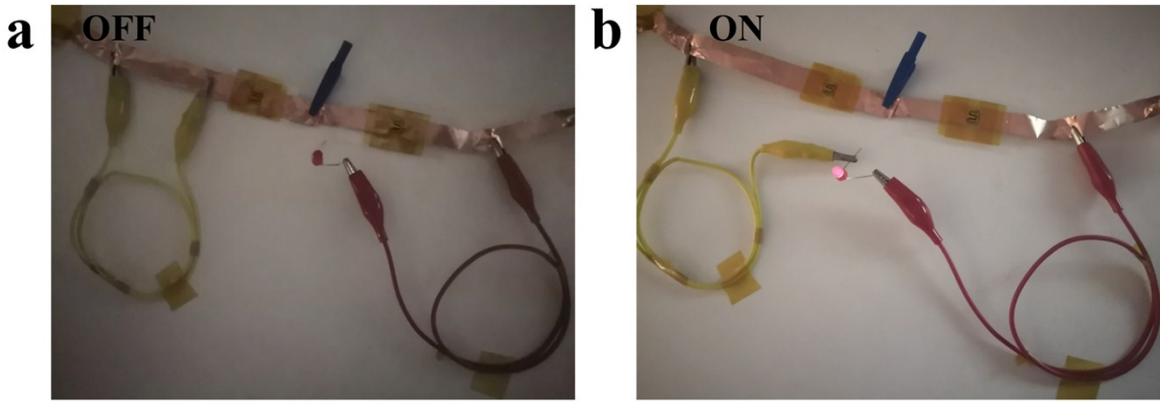

Figure S12. Photographs of a red light emitting diode (LED) powered by 2 serially-connected PNG//PNG-MoO_2-AMSCs under (a) off state and (b) on state.

Table S2. Performance comparison of PNG//PNG-MoO_2-AMSCs with other state-of-the-art MSCs.

Micro-supercapacitors (MSCs)	**Electrolyte**	**Areal Capacitance (mF cm^{-2})**	**Volumetric Capacitance (F cm^{-3})**	**Energy Density (mWh cm^{-3})**	**Power Density (W cm^{-3})**	**Refs**
PRG	PVA/H_2SO_4	1.5	233	1.5	82.7	3
SG	PVA/H_2SO_4	0.55	582	3.1	1191	4
FG	EMIMBF4/ PVDF-HFP	17.4	134	56	21	5
MXene	PVA/H_2SO_4	27	357	18	15	6
EGMX	PVA/H_2PO_4	-	62	1.4	1.6	7
MnO_2-PPy//V_2O_5-PANI	PVA/LiCl	7.26	-	19.81	2.5	8
LSG//LSG-MnO_2	Na_2SO_4	90	76	42	10	9
LIG-FeOOH//LIG-MnO_2	PVA/LiCl	21.9	5.4	2.4	2.8	10
GP/PANI-G/GP	H_2SO_4/PVA	7.63	36.8	3.14	1.1	11
LTO//AG	LiTFSI/P_{14}TFSI /PVDF-HFP	27.8	42.8	53.6	3.5	12
VN//$Co(OH)_2$	PVA/KOH	21	39.7	12.4	1.8	13
$K_2Co_3(P_2O_7)_2$//GS	PVA/KOH	0.72	6	0.96	54.5	14
NPG/MnO_2//NPG/ Ppy	PVA/LiCl	1.27	127	45.3	440	15
RGO//RGO-MoO_2	PVA-LiCl	7.9	36.2	5.46	0.16	This work
PNG//PNG-MoO_2	PVA-LiCl	33.6	152.9	38.1	0.8	This work

PRG: photochemically reduced graphene; PVA: polyvinyl alcohol; SG: sulfur-doped graphene. FG: fluorine-modified graphene. EGMX: electrochemically exfoliated graphene and MXene;

PPy: polypyrrole; PANI: polyaniline; LSG: laser-scribed graphene; LIG: laser induced graphene; GP: printable film; LTO: $Li_4Ti_5O_{12}$; AG: activated graphene; LiTFSI: bis(trifluoromethanesulfonyl)imide lithium salt; P_{14}TFSI: 1-butyl-1-methylpyrrolidinium bis(trifluoromethyl-sulfonyl)imide; PVDF-HFP: polyvinylidene difluoride-co-hexafluoropropylene; VN: vanadium nitride; GS: graphene nanosheets; NPG: nanoporous gold.

References

1. M. Baraket, S. Walton, Z. Wei, E. Lock, J. Robinson and P. Sheehan, *Carbon*, 2010, **48**, 3382-3390.
2. C. Hu, Y. Liu, Y. Yang, J. Cui, Z. Huang, Y. Wang, L. Yang, H. Wang, Y. Xiao and J. Rong, *Journal of Materials Chemistry B*, 2013, **1**, 39-42.
3. S. Wang, Z.-S. Wu, S. Zheng, F. Zhou, C. Sun, H.-M. Cheng and X. Bao, *ACS nano*, 2017, **11**, 4283-4291.
4. Z.-S. Wu, Y.-Z. Tan, S. Zheng, S. Wang, K. Parvez, J. Qin, X. Shi, C. Sun, X. Bao and X. Feng, *Journal of the American Chemical Society*, 2017, **139**, 4506-4512.
5. F. Zhou, H. Huang, C. Xiao, S. Zheng, X. Shi, J. Qin, Q. Fu, X. Bao, X. Feng and K. Müllen, *Journal of the American Chemical Society*, 2018.
6. Y.-Y. Peng, B. Akuzum, N. Kurra, M.-Q. Zhao, M. Alhabeb, B. Anasori, E. C. Kumbur, H. N. Alshareef, M.-D. Ger and Y. Gogotsi, *Energy & Environmental Science*, 2016, **9**, 2847-2854.
7. H. Li, Y. Hou, F. Wang, M. R. Lohe, X. Zhuang, L. Niu and X. Feng, *Advanced Energy Materials*, 2017, **7**, 1601847.
8. Y. Yue, Z. Yang, N. Liu, W. Liu, H. Zhang, Y. Ma, C. Yang, J. Su, L. Li and F. Long, *ACS nano*, 2016, **10**, 11249-11257.
9. M. F. El-Kady, M. Ihns, M. Li, J. Y. Hwang, M. F. Mousavi, L. Chaney, A. T. Lech and R. B. Kaner, *Proceedings of the National Academy of Sciences*, 2015, 201420398.
10. L. Li, J. Zhang, Z. Peng, Y. Li, C. Gao, Y. Ji, R. Ye, N. D. Kim, Q. Zhong and Y. Yang, *Advanced Materials*, 2016, **28**, 838-845.
11. X. Shi, Z. S. Wu, J. Qin, S. Zheng, S. Wang, F. Zhou, C. Sun and X. Bao, *Advanced Materials*, 2017, **29**, 1703034.
12. S. Zheng, J. Ma, Z.-S. Wu, F. Zhou, Y. He, F. Kang, H.-M. Cheng and X. Bao, *Energy & Environmental Science*, 2018.

13. S. Wang, Z.-S. Wu, F. Zhou, X. Shi, S. Zheng, J. Qin, H. Xiao, C. Sun and X. Bao, *npj 2D Materials and Applications*, 2018, **2**, 7.

14. H. Pang, Y. Zhang, W.-Y. Lai, Z. Hu and W. Huang, *Nano Energy*, 2015, **15**, 303-312.

15. C. Zhang, J. Xiao, L. Qian, S. Yuan, S. Wang and P. Lei, *Journal of Materials Chemistry A*, 2016, **4**, 9502-9510.